MULTIPATH DELAY ESTIMATION USING THE MAGNITUDE SPECTRUM

Granger Hickman and Jeffrey Krolik

Department of Electrical and Computer Engineering
Duke University, Durham, NC 27708

ABSTRACT

Four methods are presented by which the relative delay structure of a multipath signal can be estimated from the Fourier magnitude spectrum of the observation. The phase of the underlying source signal may be completely unknown. While the signal autocorrelation function could be used to estimate relative delay from uniform samples of the received magnitude spectrum, the novelty of the proposed methods lies in the fact that the magnitude spectrum samples are not assumed to be uniformly spaced. This makes these methods appropriate for use in frequency-hopped and collaborative sensing systems. Four methods, including a least-squares (LS), maximum likelihood (ML), maximum a posteriori (MAP), and entropy-based approach are presented. Simulation and laboratory experiments indicate that the MAP and ML algorithms provide the best performance.

1. INTRODUCTION

Multipath delay estimation is useful in a variety of radar, sonar, and communication applications. For example, in active sonar, accurate multipath delay estimation facilitates target depth estimation [1, 2]. Similarly, altitude estimation for targets acquired with over-the-horizon (OTH) radar is also dependent on an accurate assessment of the relative multipath delay in the radar return [3, 4]. However, direct delay estimation from matched-filtered, peak-detected, A-scans is seriously hampered by phase distortion due to target scattering and medium dispersion effects, which precludes simply using more signal bandwidth to improve the resolvability of the multipath in the return. Moreover, an unknown bulk delay of the return, which is treated as a nuisance parameter in this paper, adds another source of spectral phase uncertainty [2]. In this paper, the spectral distortions will be assumed to be distortions in phase only, and will be treated as non-random unknown quantities.

The magnitude spectrum of the data has desirable properties for relative delay estimation because it excludes bulk delay and target/medium induced phase distortions. At the same time, the shape of the magnitude spectrum is a function of the relative delay structure of the multipath return. In many applications, such as frequency-hopped and collaborative radar networks, only non-uniformly spaced samples of the magnitude spectrum are available. In this paper, methods that exploit non uniformly spaced magnitude spectral samples are developed.

Two of the proposed methods in this paper are based on the statistical ML and MAP techniques. The other two methods make no strong assumptions about the nature of the additive noise in the observation model. One of these is a LS technique, and the other technique is entropy-based delay estimation (EDE), which uses the entropy operator. In EDE, the ratio of the magnitude spectrum of the model replica to that of the data is maximized over the hypothesized multipath amplitudes by exploiting a special property of the entropy operator. Entropy has been used in other applications, such as SAR autofocus [5].

The proposed delay estimation methods resemble autocorrelation methods for multipath delay estimation because they are insensitive to overall phase distortions [6, 7], but are unlike them in that they do not require uniformly spaced samples from the magnitude spectrum. An important feature of these proposed methods is the fact that they assume that the multipath delays are a function of a single parameter, such as aircraft altitude or target depth. This assumption avoids the necessity of searching over a large number of dimensions when estimating the delay structure of the signal.

2. PHASE-DISTORTED OBSERVATION MODEL

For concreteness, consider an active sonar or radar application and let the Fourier-spectral data from the n^{th} observed return be denoted by $y_n(\omega_m, z, \boldsymbol{\alpha}_n)$, where ω_m is the m^{th} frequency at which the received signal spectrum is sampled, z is the depth of the target, and $\boldsymbol{\alpha}_n$ is a vector of complex scattering amplitudes weighting the linear combination of multipath returns (the k^{th} component of $\boldsymbol{\alpha}_n$ will be denoted as α_{nk}) [2-4]. The index k runs from 1 to $K_n(z)$, which is the number of transmitter-to-target-to-receiver two-way paths when the

target is at depth z. The dimension of $\boldsymbol{\alpha}_n$ is a function of the target depth, although this dependence is suppressed in the notation. Define $\tau_{nk}(z)$ as the group delay associated with the k^{th} multipath component that makes up $y_n(\omega_m, z, \boldsymbol{\alpha}_n)$, and further define

$$F_n(\omega_m, z, \boldsymbol{\alpha}_n) = \sum_{k=1}^{K_n(z)} \alpha_{nk} \exp(-j\omega_m \tau_{nk}(z)) \qquad (1)$$

Eq. (1) describes the frequency-dependent amplitude spectrum change produced by the delay structure of the multipath return and path amplitudes. Treating each return as a sum of target multipath and noise components, $y_n(\omega_m, z, \boldsymbol{\alpha}_n)$ is given by:

$$y_n(\omega_m, z, \boldsymbol{\alpha}_n) = \Theta_n(\omega_m) S(\omega_m) F_n(\omega_m, z, \boldsymbol{\alpha}_n) + \eta_n(\omega_m) \qquad (2)$$

where $\eta_n(\omega)$ represents additive noise and $S(\omega)$ is the complex spectrum of the transmitted signal. The spectral phase distortions, induced in the signal return by an uncertain bulk group delay and the target scattering function, are collectively denoted by $\Theta_n(\omega)$. The types of delay estimator that can be derived from this model is a direct function of the assumptions made about the complex ray amplitudes α_{nk}. It is assumed that the phase $\Theta_n(\omega)$ is unknown, $S(\omega)$ is known, α_{nk} is unknown, and $\tau_{nk}(z)$ is a function of the unknown target depth z. The depth dependent delays are calculated by a ray-trace algorithm with the environmental inputs appropriate to the data.

3. ENTROPY-BASED DELAY ESTIMATION (EDE)

The relative multipath delay estimation approach proposed in this section applies an entropy operator to a normalized ratio of a model magnitude spectrum to the observed magnitude spectrum, thus eliminating uncertainties present in the observed phase spectrum. The key feature of this approach is that it is sensitive to matching the peaks and nulls of the model spectrum to that of the observed spectrum. An important assumption of this approach is that the complex amplitudes α_{nk} are assumed to be non-random unknowns.

If a noiseless replica spectrum for the n^{th} observation is denoted as

$$G_n(\omega_m, z_{\text{hyp}}, \boldsymbol{\alpha}'_n) = S(\omega_m) F_n(\omega_m, z_{\text{hyp}}, \boldsymbol{\alpha}'_n) \qquad (3)$$

where z_{hyp} is a hypothesized target depth and $\boldsymbol{\alpha}'_n$ is a hypothesized vector of complex scattering amplitudes, then the following normalized ratio may be formed:

$$p_n(\omega_m, z, \boldsymbol{\alpha}'_n) = \begin{cases} \dfrac{\left| \dfrac{G_n(\omega_m, z_{\text{hyp}}, \boldsymbol{\alpha}'_n)}{y_n(\omega_m, z, \boldsymbol{\alpha}_n)} \right|^2}{\sum_{m=1}^{M} \left| \dfrac{G_n(\omega_m, z_{\text{hyp}}, \boldsymbol{\alpha}'_n)}{y_n(\omega_m, z, \boldsymbol{\alpha}_n)} \right|^2} & \text{if } \omega_m \in \Omega \\ 0 & \text{otherwise} \end{cases} \qquad (4)$$

The set of frequencies $\Omega = \{\omega_1, \ldots, \omega_M\}$ is taken to be from the support of $S(\omega)$. The ratio p_n sums to unity over the frequency argument and is non-negative, i.e., it exhibits the properties of a probability distribution. The ratio p_n will become constant over ω_m (ignoring the effects of noise) when $\boldsymbol{\alpha}'_n = \boldsymbol{\alpha}_n$ and $z_{\text{hyp}} = z$: it has the functional form of a uniform distribution. The entropy of a probability distribution $p(x_m)$, given by $H(p(x_m)) = -\sum_{m=1}^{M} p(x_m) \ln p(x_m)$, attains its maximum value when applied to a uniform distribution, which suggests the following estimate of the delay parameter z:

$$\hat{z}_{\text{EDE}} = \arg\max_{z_{\text{hyp}}} \left(\sum_{n=1}^{N} \max_{\boldsymbol{\alpha}'_n} \left(H\left(p_n(\omega_m, z_{\text{hyp}}, \boldsymbol{\alpha}'_n) \right) \right) \right) \qquad (5)$$

The maximization over $\boldsymbol{\alpha}'_n$ is achieved through a steepest-ascent gradient search. The maximization over the hypothesized depth z_{hyp} is done by a grid search. The depth estimator given in (5) is unaffected by the phase distortion $\Theta_n(\omega)$ because the function p_n is only a function of data and replica magnitude spectra. The estimator works by fitting the nulls and peaks of the replica spectrum to the data spectrum. EDE can be used for altitude or depth estimation by searching over the modeled delay sequence as a function of hypothesized altitude or depth, respectively.

4. ML DELAY ESTIMATION

Assume that the additive noise $\eta_n(\omega)$ in (2) is complex Gaussian with zero mean and variance σ^2, and also assume that the noise is uncorrelated across frequency. As was done for EDE, assume that the complex amplitudes α_{nk} are assumed to be non-random unknowns. Denote the squared-magnitude spectrum at the m^{th} frequency and n^{th} observation by $M_{mn} = |y_n(\omega_m, z, \boldsymbol{\alpha}_n)|^2$. Then M_{mn} is a scaled non-central chi-squared random variable with distribution

$$f(M_{mn};z,\boldsymbol{\alpha}_n)=\frac{1}{2\sigma^2}I_0\left(\frac{\sqrt{M_{mn}\lambda_{mn}(z)}}{\sigma^2}\right)\times \exp\left(-\frac{M_{mn}+\lambda_{mn}(z)}{2\sigma^2}\right) \quad (6)$$

where I_0 is the zero-order modified Bessel function of the first kind, and the non-centrality parameter $\lambda_{mn}(z)$ is the square of the noise-free magnitude spectrum (given in (3)):

$$\lambda_{mn}(z)=\left|G_n(\omega_m,z,\boldsymbol{\alpha}_n)\right|^2 \quad (7)$$

Denote a vector of magnitude spectrum samples for the n^{th} observation as $\mathbf{m}_n=[M_{1n},\ldots,M_{Mn}]$. Then the log-likelihood of $\mathbf{m}_n$ is given by

$$l(z_{hyp},\boldsymbol{\alpha}'_n;\mathbf{m}_n)=\sum_{m=1}^{M}\log f(M_{mn};\omega_m,z_{hyp},\boldsymbol{\alpha}'_n) \quad (8)$$

Then ML estimate of the delay parameter z, given all of the data, is expressed as

$$\hat{z}_{ML}=\arg\max_{z_{hyp}}\left(\sum_{n=1}^{N}\max_{\boldsymbol{\alpha}'_n}l\left(z_{hyp},\boldsymbol{\alpha}'_n;\mathbf{m}_n\right)\right) \quad (9)$$

The maximization over $\boldsymbol{\alpha}'_n$ for a given value of z_{hyp} is achieved by a gradient ascent algorithm, and the maximization over z_{hyp} is done by a grid search.

5. MAP DELAY ESTIMATION

The MAP delay estimator is derived by making the same assumptions about the noise, $\eta_n(\omega)$, as was made for the ML delay estimator, and by also assuming that the complex amplitudes $\boldsymbol{\alpha}_n$ are complex Gaussian with zero mean and known covariance matrix $\mathbf{R}_n$. Then the joint log-density of $\mathbf{m}_n$ and $\boldsymbol{\alpha}_n$ is given by

$$h(\mathbf{m}_n,\boldsymbol{\alpha}_n;z)=\log\sum_{m=1}^{M}f(M_{mn};\omega_m,z,\boldsymbol{\alpha}_n) - \log\det\mathbf{R}_n-\boldsymbol{\alpha}_n^H\mathbf{R}_n^{-1}\boldsymbol{\alpha}_n \quad (10)$$

It follows that estimator of the delay parameter z, given all of the data, is given by

$$\hat{z}_{MAP}=\arg\max_{z_{hyp}}\left(\sum_{n=1}^{N}\max_{\boldsymbol{\alpha}'_n}h\left(\mathbf{m}_n,\boldsymbol{\alpha}'_n;z_{hyp}\right)\right) \quad (11)$$

Notice that that this estimate employs a MAP estimate of the complex amplitudes $\boldsymbol{\alpha}_n$ for each hypothesized value of z_{hyp}. The mechanics of the optimization procedure for the expression (11) is essentially unchanged from that for the ML estimator in the previous section.

6. LS DELAY ESTIMATION

The derivation of the LS delay estimator hinges, as did the derivation of EDE, on the assumption that the complex amplitudes $\boldsymbol{\alpha}_n$ are non-random unknowns. Another similarity is the fact that no particular distribution is assumed for the additive noise $\eta_n(\omega)$.

The square error between the n^{th} magnitude spectrum and the replica spectrum resulting from the hypothesized amplitudes $\boldsymbol{\alpha}'_n$ and delay parameter z_{hyp}, accumulated across frequency, is

$$Q\left(z_{hyp},\boldsymbol{\alpha}'_n,\mathbf{m}_n\right)=\sum_{m=1}^{M}\left(M_{mn}-\lambda_{mn}(z_{hyp})\right)^2 \quad (12)$$

The LS estimate of the delay parameter is then

$$\hat{z}_{LS}=\arg\min_{z_{hyp}}\left(\sum_{n=1}^{N}\min_{\boldsymbol{\alpha}'_n}Q\left(z_{hyp},\boldsymbol{\alpha}'_n;\mathbf{m}_n\right)\right) \quad (13)$$

Just as for the other delay estimators in this paper, minimization over $\boldsymbol{\alpha}'_n$ for a given value of z_{hyp} is achieved by a gradient descent algorithm, and the minimization over z_{hyp} is done by a grid search.

7. RESULTS

The estimators in this paper have been applied to real electromagnetic data gathered under laboratory conditions which were designed to mimic a simple multipath radar or sonar scenario with four paths between the transmitter and receiver. The data was generated by using a network analyzer with transmit and receive antennas attached to its input and output ports. The broadcast radiation was scattered from a cylindrical target placed near a flat reflector. Radiation-absorbing panels were placed around the periphery of the experimental setup in order to reduce undesirable scattering from other objects in the laboratory. The actual specifications of the geometry are summarized in Fig. 1. The transmitter and receiver have z

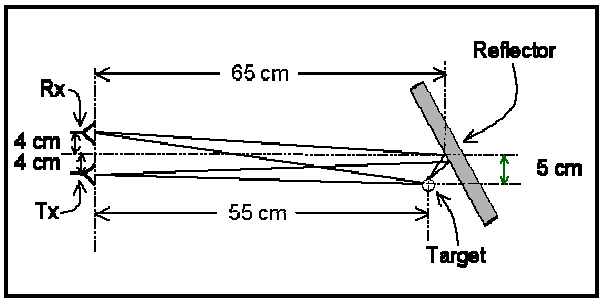

Fig. 1. Schematic of the lab experiment as seen from above.

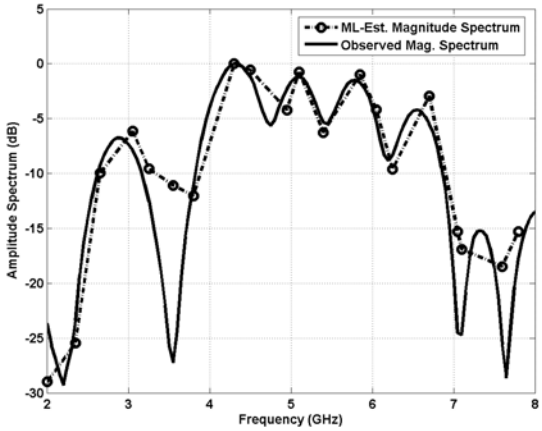

Fig. 2. Comparison of the observed magnitude spectrum (solid line) to the model spectrum (dashed line, circle marker) that results when the complex amplitudes are estimated via the gradient ascent algorithm used with the ML delay estimator. Note that the model frequency samples are not uniformly distributed.

coordinates of –4 cm and +4 cm, respectively, and both have x coordinates of 0 cm. The reflector crosses the x-axis at 65 cm at an angle of 60 degrees, measured clockwise from the x-axis to the reflector front surface.

The steel cylindrical target was 5.7 cm in diameter, and its center had an x coordinate of 55 cm and a z coordinate of –5 cm. The transmitted signal had significant energy in the 0.5 GHz to 10.5 GHz band, but only the band between 2 GHz and 8 GHz was actually used in the estimation calculations. The shortest wavelength of radiation used, 3.75 cm, is on the order of the diameter of the cylinder, which is also true for the OTH radar altitude estimation problem.

The transmitted signal had a duration of 0.5 ns and the received signal was sampled at 40 GHz. The length of the sampled time-domain signal was 20 ns, or 801 samples. Thus, adjacent discrete Fourier transform (DFT) samples are spaced 50 MHz apart. Out of the 120 bins in the 2 to 8 GHz frequency band, only 20 were used

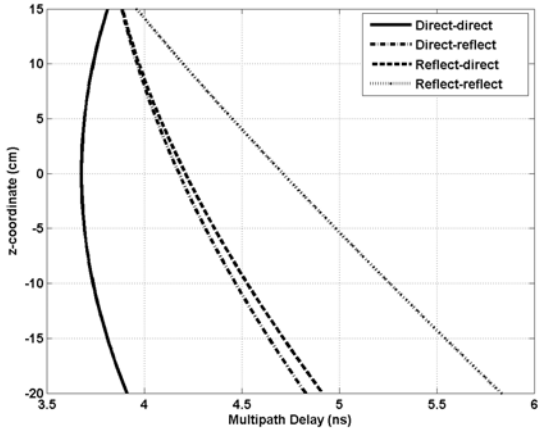

Fig. 3. Multipath delays as a function of target displacement when a point target is assumed.

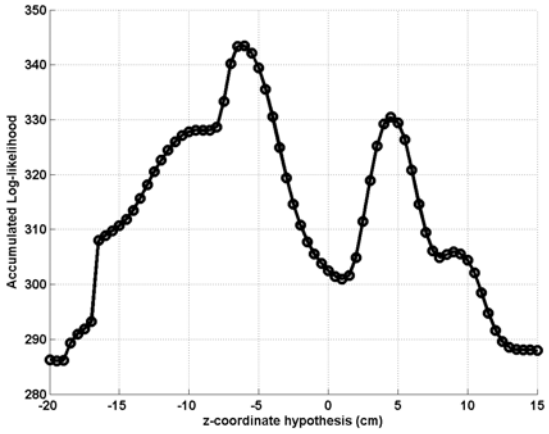

Fig. 4. Cumulative log-likelihood versus the hypothesized target displacement. The ML estimate is 6 cm and the true displacement is 5 cm

for delay estimation, and they were chosen so that the inter-bin spacing was not constant across the band. This is illustrated in Fig. 2, which compares an ML-estimated spectrum to the observed magnitude spectrum. The transmitter antenna was designed to confine the majority of the broadcast radiation to a horizontal plane. The resulting scattering from the cylindrical target, which has its axis of symmetry perpendicular to this horizontal plane, can be described by a two-dimensional model. Thus, the localization problem takes place in an essentially two-dimensional space, with horizontal coordinate x and vertical coordinate z.

The delay estimation algorithms proposed earlier in this paper were applied to the problem of localizing the target's z coordinate, while all other dimensions were assumed known, except for the target radius. The resulting delay structure as a function of hypothesized z coordinate is shown in Fig. 3. A plot of log-likelihood vs.

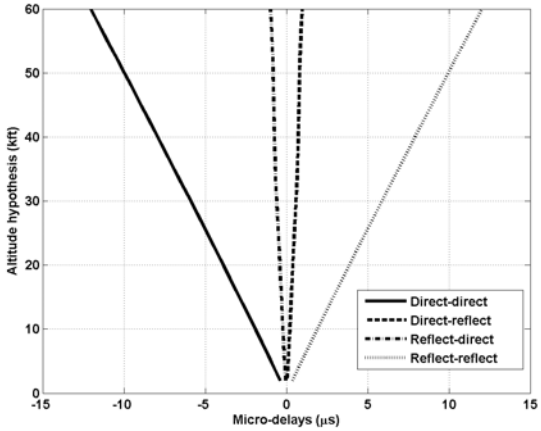

Fig. 5. Path delay as a function of altitude for an example environment.

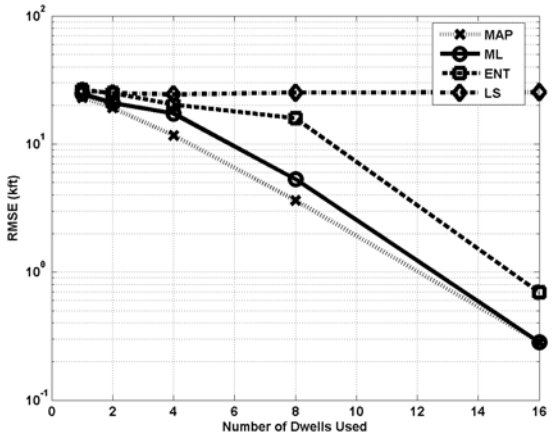

Fig. 6. Monte Carlo estimates of RMSE for each estimator as a function of the number of dwells. The SNR was 10 dB, the true altitude was 10 kft, and 100 trials were used for each RMSE estimate.

hypothesized z coordinate is shown in Fig. 4. The resulting ML estimate of the z coordinate is –6 cm (true z coordinate was –5 cm). Similar results were calculated with the MAP, LS, and entropy-based estimators: the estimated z coordinates were –5.5 cm, -6.0 cm, and –6.0 cm, respectively.

Since this laboratory data was at a very high SNR (approximately 80 dB), the performance of the four estimators was largely driven by mismatch problems, such as unsuppressed extraneous scattering and inaccurate propagation modeling due to the assumption that the target was a point target. In order to test these estimators under more closely controlled conditions, simulations of a broad-band OTH radar experiment were performed. The multipath delays are a function of altitude, and a plot of the delays versus altitude is shown in Fig. 5. The transmitted signal had a flat spectrum over a 1 MHz bandwidth, and the observed magnitude spectrum consisted of 15 samples at frequencies that were not uniformly spaced.

Fig. 6 shows the estimated root-mean square error (RMSE) performance of the ML, MAP, entropy, and LS estimators as a function of the number of magnitude spectra observations used. The target altitude and signal SNR were fixed to 10 kft and 10 dB, respectively, in all cases. The number of magnitude spectra used was allowed to take on the values 1, 2, 4, 8, and 16. For each RMSE estimate, 100 realizations were used. All estimates improve with more data, except for the LS estimator, which indicates that the LS estimator is operating below threshold and large errors are spoiling its performance.

Fig. 7 demonstrates the estimated RMSE performance as a function of target altitude, where the SNR was fixed to 10 dB, eight magnitude spectra per estimate were used, and 100 estimates were used per RMSE estimate. For each estimator, the RMSE decreases with increasing altitude. This occurs because the delay spread increases with altitude (see Fig. 5), which implies that the interference pattern caused by the complex exponentials in (1) oscillates more rapidly over the bandwidth of the received signal, making it easier for the algorithms to discern the interference pattern overlaying the transmitted signal magnitude spectrum. As the target altitude goes lower, the peaks and nulls induced by the complex exponential interference are farther apart, until, finally, they are masked by noise. As in the previous example, the LS estimator is the worst performer; the RMSE for the LS estimator here is practically equal to the RMSE that would be expected if the LS estimates were uniformly distributed over the altitude grid, which indicates that large errors are dominating the performance of the estimator. The other estimators are ranked as before, with the entropy estimator performing worse than the ML estimator, and the MAP estimator performing the best. Note that the performance of all other estimators degrades more rapidly than that of the MAP estimator, which assumes more prior knowledge about the multipath amplitudes.

Fig. 8 shows the estimated RMSE performance of the estimators as a function of SNR. The altitude of the target was fixed to 10 kft. Note that the LS estimator begins to show improvement above 10 dB SNR, achieving performance at 25 dB approximately equal to that of the MAP estimator at 10 dB, and to that of the entropy estimator at 15 dB. When the SNR exceeds 15 dB, the RMSE estimates for the MAP and ML estimators go to zero, which is due to the fact that the RMSE of these estimators is much smaller than the 2 kft altitude grid sampling interval.

8. CONCLUSION

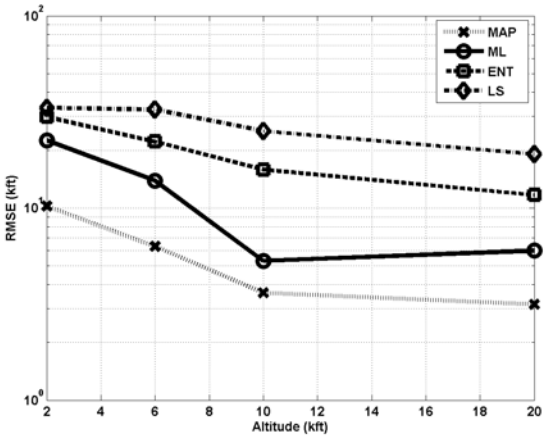

Fig. 7. Monte Carlo estimates of RMSE for each estimator as a function of the target altitude. The SNR was 10 dB, 8 observations were used for each trial, and 100 trials were used for each RMSE estimate.

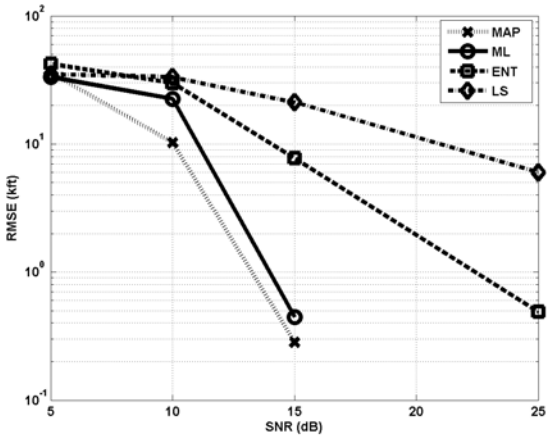

Fig. 8. Monte Carlo estimates of RMSE for each estimator as a function of the target altitude. The true altitude was 10 kft, 8 observations were used for each trial, and 100 trials were used for each RMSE estimate.

This paper has presented four delay estimation techniques (MAP, ML, entropy, and LS) which can be interpreted as attempts to match the frequency-domain interference pattern seen in the magnitude spectrum to a delay hypothesis. The various estimators arise from different assumptions about the multipath amplitudes and the additive noise, with the MAP estimator being the most restrictive and the entropy and LS estimators the least restrictive in their assumptions.

The estimators were successfully applied to a real data example using electromagnetic data gathered in a laboratory. The performance of the estimators was also explored in simulation, focusing on their behavior relative to changes in delay spread (through altitude change), SNR, and amount of data used to form an estimate. It is shown through simulation that the MAP estimator performs the best, followed by the ML estimator, the entropy estimator, and then the LS estimator.

One advantage of these techniques is that they can be applied to problems where the broad-band magnitude spectrum can be only be partially sampled, and not necessarily uniformly sampled, as would be required by a direct application of the autocorrelator delay estimator. This is useful, for example, for application to scenarios that are constrained to use narrow-band signals in order to both mitigate interference with other users and avoid known interferers.

ACKNOWLEDGMENTS

This work was supported by the Office of Naval Research under grants no. N00014-05-10023 and N00014-03-1-0041.

REFERENCES

[1] T. C. Yang and T. W. Yates, "Scattering from an object in a stratified medium. I. frequency dispersion and active localization," *J. Acoust. Soc. Am.* **96**, pp. 1003-1019 (1994).

[2] G. Hickman and J. Krolik, "Matched-field depth estimation for active sonar", *J. Acoust. Soc. Am* **115**, (2004).

[3] M. Papazoglou and J. Krolik, "Matched field estimation of aircraft altitude from multiple over-the-horizon radar revisits," *IEEE Trans. Signal Process.* **47**, pp. 966-976, (1999).

[4] M. Papazoglou and J. Krolik, "Estimation of aircraft altitude and altitude rate with over-the-horizon radar," *ICASSP Proc.*, pp. 2103-2106, (1999).

[5] A. Yegulalp, "Maximum entropy SAR autofocus," ASAP 1999 Workshop, MIT Lincoln Labs, March 1999.

[6] J. O. Smith and Friedlander, "Adaptive multipath delay estimation," *IEEE Trans. ASSP* **33**, pp.812-822, (1985).

[7] P. P. Moghaddam, H. Amindavar, and R. L. Kirlin, "A new time-delay estimation in multipath," *IEEE Trans. ASSP* **51**, pp.1129-1141, (2003).